Biogeosciences, 22, 4433–4448, 2025
https://doi.org/10.5194/bg-22-4433-2025

Biogeosciences Open Access EGU

Variations in vegetation evapotranspiration affect water yield in high-altitude areas

Yinying Jiao[1,2,3], Guofeng Zhu[1,2,3], Dongdong Qiu[4], Siyu Lu[1,2,3], Gaojia Meng[1,2,3], Rui Li[1,2,3], Qinqin Wang[1,2,3], Longhu Chen[1,2,3], and Wentong Li[1,2,3]

[1]College of Geography and Environment Science, Northwest Normal University, Lanzhou 730070, Gansu, China
[2]Shiyang River Ecological Environment Observation Station, Northwest Normal University, Lanzhou 730070, Gansu, China
[3]Key Laboratory of Resource Environment and Sustainable Development of Oasis, Gansu Province, Lanzhou 730070, Gansu, China
[4]School of Atmospheric Sciences, Nanjing University, Nanjing 210000, Jiangsu, China

Correspondence: Guofeng Zhu (zhugf@nwnu.edu.cn)

Received: 17 July 2024 – Discussion started: 19 August 2024
Revised: 4 June 2025 – Accepted: 2 July 2025 – Published: 8 September 2025

Abstract. Global mountains and plateaus are the main water-producing areas on land. However, under the influence of climate change, the distribution of vegetation and the way water is utilized in these areas have undergone significant changes. As such, understanding the effects of evapotranspiration from high-altitude vegetation on precipitation and runoff is vital in addressing the uncertainties and challenges posed by climate change and anthropogenic transformation. The stable isotopes in waterbodies play a crucial role in determining the evapotranspiration capacity of ecosystems and the mechanisms of precipitation formation. Between 2018 and 2022, we conducted research in the northeastern Qinghai–Tibet Plateau, collecting and analysing stable isotope water data from precipitation, soil water, and *Picea crassifolia* xylem water to quantify the impact of vegetation transpiration and recirculated water vapour on precipitation. Our findings indicate that transpiration from vegetation accounts for the largest share of evapotranspiration within the entire forest ecosystem, averaging 57 %. Therefore, vegetation transpiration is the decisive factor in determining the water yield of inland high-altitude areas. Local evapotranspiration contributes an average of 28 % to precipitation, further enhancing the replenishment of precipitation in high-altitude areas. The warming of global temperatures and human activities are likely to induce shifts in the distribution areas and evapotranspiration regimes of alpine vegetation, potentially altering water resource patterns in the basin. It is necessary to actively adapt to the changes in water resources in the inland river basin.

1 Introduction

Projected future scenarios suggest that drought events will become more frequent, severe, and prolonged due to the effects of climate change. This phenomenon is expected to manifest most rapidly and intensely in arid and semi-arid regions (Ault, 2020). Large-scale forest ecosystems play a pivotal role in influencing climate through biophysical feedback mechanisms and in altering the global water cycle. The stable hydrogen and oxygen isotopes found in precipitation, plant water, and soil water can effectively trace evaporation within the water cycle. During water evaporation, isotopic fractionation occurs as molecules of differing mass are redistributed between the vapour and liquid phases, leaving heavier isotopes such as D and $\delta^{18}O$ predominantly in the liquid phase (Dansgaard, 1964). Plant transpiration further enriches heavy isotopes in leaf water, while the heavier and lighter molecules released through stomata remain in equilibrium with the xylem water supply. This mechanism underpins the use of stable isotopes to estimate vegetation transpiration capacity (Farquhar et al., 2007). The *Picea crassifolia* ecosystem, providing a range of ecological, climatic, and social benefits to the northeastern Qinghai–Tibet Plateau, exhibits high susceptibility to drought and temperature extremes. Fur-

thermore, climate-related drivers significantly heighten the vulnerability of *Picea crassifolia* to drought and heat stress, with an anticipated increase in disturbances to its ecosystem as climate change progresses.

Variations in evaporation loss are known to precipitate disturbances in the precipitation and surface water budget (Li et al., 2023). Furthermore, forest evapotranspiration (ET) significantly influences atmospheric moisture convergence and precipitation dynamics, with its impact critically dependent on ambient moisture conditions (Makarieva et al., 2023). Additionally, across different spatial scales, vegetation transpiration capacity and local water availability demonstrate complex and variable relationships. This is specifically reflected in the following aspects. Enhanced evapotranspiration can contribute up to 45 % of available water in both local and downwind regions, though this proportion may substantially vary in water-scarce environments (Cui et al., 2022). As precipitation recycling and moisture convergence intensify, the sensitivity of precipitation to evapotranspiration becomes increasingly pronounced (Cheng et al., 2024). In regions characterized by high vegetation cover and elevated topography, moisture recycling significantly enhances regional water resource availability (An et al., 2025). The upward movement of water vapour in the atmosphere, upon merging with advection water vapour, condenses to form precipitation. Consequently, in high-altitude areas with greater vegetation coverage and favourable conditions for moisture convergence, precipitation is typically more abundant. The trajectory and intensity of westerly winds critically determine moisture content and precipitation distribution across Central Asian mountain ranges, particularly during the cold season under the substantial influence of the subtropical westerly jet (Mehmood et al., 2022). Even minor redistributions of atmospheric water can trigger significant cascading effects, inducing substantial shifts in latent heat flux, atmospheric circulation, water transport mechanisms, and precipitation patterns (Hao et al., 2023). Moreover, for high-altitude regions influenced by the cryosphere, the mechanism by which vegetation-dominated water vapour contributes to precipitation and runoff formation remains a critical knowledge gap.

As a vascular plant species, *Picea crassifolia* plays a crucial role in channelling energy and materials from the environment into terrestrial ecosystems. Its growth, survival, and reproduction significantly influence the ecological functions and structures of other species, both within their habitats and in broader ecological contexts. A significant interaction exists between the vegetation, its drought resilience, and the microclimatic conditions within forests and their ecosystems. This interaction is vital for understanding ecosystem dynamics (Eisenhauer and Weigelt, 2021). In this study, we conducted monthly observations and analyses of the xylem water potential, soil water potential, stable isotopes of precipitation, and soil water content of *Picea crassifolia* in the northeastern Qinghai–Tibet Plateau from April to October for the years 2018 and 2022. These data were utilized to address the following research objectives: (1) to quantify the contribution rates of soil evaporation and vegetation transpiration to the total evapotranspiration of ecosystems, (2) to determine the ratio of recirculated water vapour in precipitation, and (3) to investigate the evapotranspiration process and its impact on productivity and hydrological convergence in the forest belt of the mountainous region. This study provides a robust foundation for the management of local water resources and the protection of ecological integrity.

2 Study area

The Qilian Mountains are located in the central part of the Eurasian continent, on the northeastern edge of the Qinghai–Tibet Plateau (Fig. 1). The eastern region is dominated by water erosion, with large variations in mountainous terrain and an average elevation of over 4000 m. Permafrost is developed at elevations of 3500 to 3700 m, and areas above 4500 m are characterized by modern glacier development. The region has a plateau continental climate, with hot summers and cold winters, strong solar radiation, and large temperature differences between day and night. The average annual temperature is below 4 °C, with extreme highs of 37.6 °C and extreme lows of −35.8 °C. The annual sunshine hours range from 2500 to 3300 h, with total solar radiation of 5916 to 15 000 MJ m^{-1}. The average annual precipitation is 400 mm, and the annual evaporation ranges from 1137 to 2581 mm. The average wind speed is around 2 m s^{-1}, and the frost-free period lasts from 23.6 to 193 d. The Shiyang River originates from the Daxueshan on the northern side of the Lenglong Ridge in the eastern section of the Qilian Mountains, serving as a major water source for the city of Wuwei. The soil types in the eastern section are diverse but with low organic matter content. The distribution of vegetation shows distinct zonal characteristics, with mountainous forest–grassland zones (2600 to 3400 m), subalpine shrub–meadow zones (3200 to 3500 m), and high-mountain subice–snow sparse-vegetation zones (> 3500 m) at elevations above 2700 m. The main types of natural forest vegetation include *Picea crassifolia*, Qilian juniper forest, and Chinese pine forest, with *Picea crassifolia* being the dominant tree species (Zhu et al., 2022b).

3 Materials and methods

3.1 Material sources

In this study, we established a stable isotope observation network at four elevation zones (2543, 2721, 3068, 3448 m) in terms of vertical height (Table 1). Meteorological data were recorded using an automatic weather station in the years 2018 and 2022. The collected precipitation was subsequently transferred to 100 mL containers following each rainfall event. Soil samples were extracted from the sample

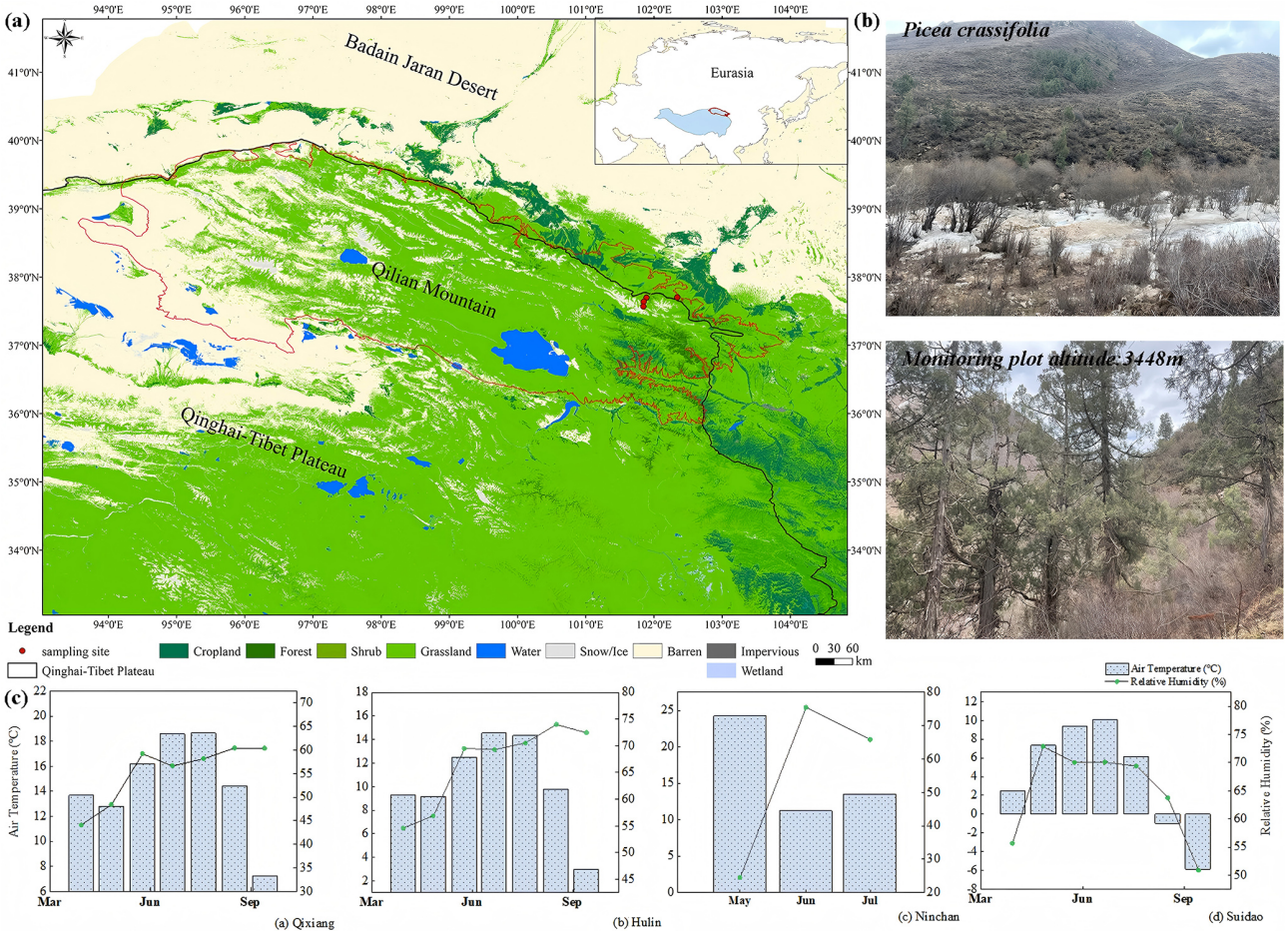

Figure 1. Overview of the study area. **(a)** Geographical location of the study area, **(b)** growth status of *Picea crassifolia*, and **(c)** seasonal variation in meteorological conditions.

plot at various depths, specifically at intervals of 0–5, 5–10, 10–20, 20–30, 30–40, 40–50, 50–60, 60–70, 70–80, 80–90, and 90–100 cm, utilizing a soil drill. These samples were bifurcated, with one portion being stored in a 50 mL glass bottle. This bottle was hermetically sealed with a parafilm and transported to the observation station, where it was marked with the sampling date and subjected to cryopreservation within 10 h for the purpose of stable isotope analysis. The remaining portion of the soil sample was placed in a 50 mL aluminium box to ascertain soil water content through a drying method. For the collection of plant samples, scissors were employed to harvest the xylem stems of vegetation. The bark was removed, and the samples were placed in 50 mL glass bottles, which were then sealed and frozen for subsequent experimental analysis.

Surface evapotranspiration data at an elevation of 2700 m were sourced from the MODIS-based daily surface evapotranspiration dataset for the Qilian Mountains. Evapotranspiration data at 3200 m were obtained from high-quality literature that includes field-observed ET values within the elevation range of 2500 to 3400 m to reinforce our research findings. Precipitation data at different elevations were all sourced from the National Tibetan Plateau Data Center.

3.2 Experimental analysis

The isotopic data used in this study mainly include stable isotopes of precipitation, soil water, and xylem water. All isotopic samples were analysed at the Stable Isotope Laboratory of Northwest Normal University. The precipitation samples were analysed for hydrogen and oxygen stable isotopes using a liquid water isotope analyser (DLT-100, Los Gatos Research, USA). After thawing the soil and vegetation samples, they were extracted using a low-temperature vacuum condensation device (LI-2100, LICA United Technology Limited, China), and the extracted water was subjected to isotopic analysis. Each water sample was tested six times to ensure accuracy, with the first two tests considered interference, and only the results of the subsequent four tests were averaged (Zhu et al., 2022a). The isotopic measurements are represented by δ, which denotes the deviation in parts per thousand of the ratio of two stable isotopes in the sample

Table 1. Sampling location, the meteorological background, and sampling quantity information during the growing season.

Parameter	Station	Qixiang	Hulin	Ninchan	Suidao
Altitude (m)		2543	2721	3068	3448
Local climate	Temperature (°C)	3	3.2	3.3	−0.9
	Precipitation (mm)	262	370	394	475
	Relative humidity (%)	52.9	56.1	66.6	69.2
Number of samplings	Precipitation	53	108	91	135
	Soil water	220	560	560	560
	Xylem water	236	56	56	56

relative to the ratio in a standard sample. The International Atomic Energy Agency (IAEA) defined the Vienna Standard Mean Ocean Water (VSMOW) in 1968 as the standard for isotopic composition, which is derived from distilled seawater and has a similar isotopic composition to Standard Mean Ocean Water (SMOW).

$$\delta = \left(\frac{\delta_{\text{Sampling}}}{\delta_{\text{Standard}}} - 1\right) \times 1000‰ \quad (1)$$

3.3 Research methods

First, determining the isotopic composition of water vapour formed from precipitation, vegetation, and soil evaporation serves as the foundation for applying different models. Based on the isotopic values of different water vapour sources, the contribution of vegetation's evapotranspiration to the overall ecosystem evaporation can be established, which is a step in identifying the key factors affecting precipitation. Next, an end-member mixing model is used to quantify the contribution ratio of recycled water vapour in precipitation. The results of this analysis will be used to assess the impact of these key factors on the formation of precipitation. The parameters involved in the methods are all listed in Table S1 in the Supplement.

3.3.1 Isotopic composition of atmospheric water vapour

The stable isotope composition of moisture in ambient air (δ_a) is calculated as follows (Gibson and Reid, 2014; Skrzypek et al., 2015):

$$\delta_a = \frac{\delta_{\text{rain}} - k\varepsilon^+}{1 + k\alpha^+ \times 10^{-3}}, \quad (2)$$

where $k = 1$ or, by fitting k to some fraction of 1 as the best fit to the local evaporation line, ε^+ is the isotopic fractionation factor, defined by $\varepsilon^+ = (\alpha^+ - 1) \times 1000$. α^+ for ^{2}H and ^{18}O are calculated as follows (Horita and Wesolowski, 1994):

$$\begin{aligned} 10^3 \ln^2\alpha^+ &= 1158.8T^3/10^9 - 1620.1T^2/10^6 \\ &\quad + 794.84T/10^3 - 161.04 \\ &\quad + 2.9992 \times 10^9/T^3, \end{aligned} \quad (3)$$

$$\begin{aligned} 10^3 \ln^{18}\alpha^+ &= -7.685 + 6.7123 \times 10^3/T \\ &\quad - 1.6664 \times 10^6/T^2 + 0.35041 \times 10^9/T^3. \end{aligned} \quad (4)$$

Here, α^+ is the equilibrium fractionation factor dependent on temperature and T is the temperature (K). The value of α^+ is usually around 1.01, and the value of ε^+ is typically around 10.

3.3.2 Isotopic composition of soil evaporation

The Craig–Gordon model was used to calculate the stable isotopic composition of soil evaporation water vapour, δ_E, using the following equation (Yepez et al., 2005):

$$\delta_E = \frac{\alpha_e^{-1}\delta_s - h\delta_a - \varepsilon_{eq} - (1-h)\varepsilon_k}{(1-h) + 10^{-3}(1-h)\varepsilon_k}, \quad (5)$$

where $\alpha_e (> 1)$ is the equilibrium factor calculated as a function of water surface temperature, δ_S is the stable isotopic composition of liquid water at the evaporating surface of the soil (0–10 cm average stable isotopic composition of soil water), δ_a is the stable isotopic composition of atmospheric water vapour near the surface, ε_{eq} represents the equilibrium fractionation corresponding to $\varepsilon_{eq} = (1 - 1/\alpha_e) \times 1000$, ε_k is the kinetic fractionation factor of oxygen and is approximately 18.9‰, and h is the atmospheric relative humidity (Gibson and Reid, 2009). For δ^{18}O, α_e is calculated as follows (Raz-Yaseef et al., 2010):

$$\alpha_e = \frac{1.137 \times 10^6/T^2 - 0.4156 \times 10^3/T - 2.0667}{1000} + 1, \quad (6)$$

where T is the soil temperature (K) at a depth of 5 cm.

3.3.3 Isotopic composition of plant transpiration

When transpiration is strong, leaf water is in "isotopic stable state"; that is, the isotopic composition of leaf transpiration water is equivalent to that of water absorbed by the roots

of rain plants at noon. Therefore, the stable isotopic composition of water in plant xylem can be used to represent the stable isotopic composition of water vapour in plant transpiration. The expression is as follows (Aron et al., 2020):

$$\delta_{\mathrm{T}} = \delta_X, \tag{7}$$

where δ_X is the isotopic ratio of xylem water and δ_{T} is the isotopic ratio of transpiration.

3.3.4 Evapotranspiration isotope assessment

The Keeling plot model describes the linear relationship between the oxygen isotope composition of atmospheric water vapour and its reciprocal concentration. The intercept of the curve on the y axis represents the oxygen isotopic composition of evapotranspiration (δ_{ET}) and is expressed as follows (Keeling, 1958; Wang et al., 2015):

$$\delta_{\mathrm{a}} = \frac{C_{\mathrm{b}}(\delta_{\mathrm{b}} - \delta_{\mathrm{ET}})}{C_{\mathrm{a}}} + \delta_{\mathrm{ET}}, \tag{8}$$

where δ_{a} and C_{a} represent the atmospheric water vapour oxygen isotopic composition (‰) and water vapour concentration in the ecosystem boundary layer, δ_{b} and C_{b} represent the background atmospheric water vapour oxygen isotopic composition and background atmospheric water vapour concentration, and δ_{ET} is the ecosystem evapotranspiration oxygen isotopic composition.

3.3.5 Proportion of vegetation transpiration

The determination of evapotranspiration by means of biotic and abiotic isotopic composition can be used to improve the understanding of community structure and ecosystem function in *Picea crassifolia* in the northeast of the Qinghai–Tibet Plateau. Based on the isotope mass balance approach to consider the distribution of major and minor isotopes, the partitioning of evapotranspiration can be achieved using two end-member mixing models (E and T) with the following expression (Kool et al.,2014; Wei et al., 2018):

$$\frac{T}{\mathrm{ET}} = \frac{\delta_{\mathrm{ET}} - \delta_E}{\delta_T - \delta_E}, \tag{9}$$

where δ_{ET}, δ_E, and δ_T are the isotopic compositions of evapotranspiration (ET), soil evapotranspiration (E), and plant evapotranspiration (T), respectively, and the isotopic values of the three can be obtained by both direct observation and model estimation.

3.3.6 Bayesian mixing model

Assuming that precipitation vapour is a mixture of advective water vapour and recirculating water vapour, it is understood that the proportions of both precipitation and precipitation water vapour have the same nature. The proportion of precipitation occupied by recycled vapour is calculated as follows (Kong et al., 2013; Wang et al., 2022):

$$f_{\mathrm{re}} = \frac{P_{\mathrm{tr}} + P_{\mathrm{ev}}}{P_{\mathrm{tr}} + P_{\mathrm{ev}} + P_{\mathrm{adv}}} = f_{\mathrm{tr}} + f_{\mathrm{ev}}, \tag{10}$$

where P_{tr}, P_{ev}, and P_{adv} are precipitation produced by transpiration, surface evaporation, and advection, respectively. The relationships among these three types of water vapour and precipitation are as follows (Brubaker et al., 1993; Sang et al., 2023):

$$\delta_{\mathrm{pv}} = \delta_{\mathrm{tr}} f_{\mathrm{tr}} + \delta_{\mathrm{ev}} f_{\mathrm{ev}} + \delta_{\mathrm{adv}} f_{\mathrm{adv}}, \tag{11}$$

$$f_{\mathrm{ev}} + f_{\mathrm{tr}} + f_{\mathrm{adv}} = 1, \tag{12}$$

where f_{tr}, f_{ev}, and f_{adv} are the proportional contributions of transpiration, surface evaporation, and advection, respectively, to precipitation. The f values of three kinds of water vapour were obtained by ISOSource software (https://www.epa.gov/, last access: 16 April 2025) (Phillips and Gregg, 2001). δ_{pv}, δ_{tr}, δ_{ev}, and δ_{adv} represent the stable isotopic compositions of precipitation vapour, vegetation transpiration vapour, water surface evaporation vapour, and advected vapour, respectively. δ_{pv} is calculated using the following formula:

$$\delta_{\mathrm{pv}} = \frac{\delta_{\mathrm{p}} - k\varepsilon^+}{1 + k\varepsilon^+}, \tag{13}$$

where δ_{p} represents the stable isotopic composition of precipitable liquid water.

Based on the isotopic relationships among different water phases in either open or closed isotope systems, we use the isotope evaporation model proposed by Craig and Gordon (1965) to determine the stable isotopic composition of soil evaporation vapour (δ_{ev}). The equation is as follows:

$$\delta_{\mathrm{ev}} = \frac{\delta_{\mathrm{s}}/\alpha^+ - h\delta_{\mathrm{adv}} - \varepsilon}{1 - h + \varepsilon_k}, \tag{14}$$

where δ_{s} is the isotopic composition of the liquid water evaporation front, δ_{adv} is advective vapour, h is relative humidity, α^+ is the equilibrium fractionation factor, ε_k is the kinetic fractionation factor, and ε is the total fractionation factor.

$$\varepsilon = \varepsilon^+/\alpha^+ + \varepsilon_k, \tag{15}$$

$$\varepsilon_k = (1 - h)\theta_n C_{\mathrm{k}}, \tag{16}$$

where h is the relative humidity C_{k} is the kinetic fractionation constant; δ^2H is 25.1 ‰, and δ^{18}O is 28.5 ‰. The weight coefficient θ of a small waterbody is 1, and θ of a large waterbody is 0.5. n ranges from 0.5 (fully turbulent transport, with reduced kinetic fractionation, suitable for lake or saturated soil conditions) to 1 (fully diffused transport, suitable for very dry soil conditions), with a kinetic fractionation coefficient of about 12.2 ‰–24.5 ‰ for ε_k (^{2}H) in a dry atmosphere ($h = 0$). The kinetic separation coefficient of ε_{k} (^{18}O) is about 13.8 ‰–27.7 ‰.

The advection water vapour isotope δ_{adv} in the three-component mixing model needs to be determined by the water vapour isotopic composition at the upwind position. The HYSPLIT model (http://www.arl.noaa.gov/ready/HYSPLIT.html, last access: 16 April 2025), designed for atmospheric transport analysis using gridded meteorological data, was applied to track moisture sources and analyse air mass trajectories to sampling locations (Stein et al., 2015). We found that the northeast of the Qinghai–Tibet Plateau was controlled by westerly winds, the southeast monsoon, and the plateau monsoon in June, July, and August and by prevailing westerly winds in September and October. The clustering analysis of air masses in different months shows that air masses accumulate at the northern foot of the Qilian Mountains and move from low altitude to high altitude along the valley. Xiying, at 2097 m above sea level, is therefore used as an upwind station from April to October (Zhang et al., 2021). As the air mass ascends along the elevation gradient from this station, the isotope of advective vapour is progressively depleted. Notably, although recycled vapour produced by evapotranspiration does enter the air mass to some extent, most of it escapes to other regions without contributing to precipitation. Consequently, its influence on advective vapour downwind can be considered negligible (Li and Zhang, 2003; Wang et al., 2016). Because this transport process is irreversible and departs from isotopic mass balance in the atmosphere, isotopic fractionation is assumed to be due to Rayleigh distillation (Peng et al., 2011), which is formulated as follows:

$$\delta_{adv} = \delta_{pv-adv} + (\alpha^{+} - 1)\ln F, \quad (17)$$

where δ_{pv-adv} denotes the isotopic composition of precipitable water vapour at the upwind station, which is obtained from Eq. (13). The parameter F primarily reflects atmospheric moisture conditions during regional precipitation formation and is commonly represented by the ratio of final to initial water vapour. Since water vapour content is positively correlated with the surface vapour pressure of the whole study area ($c = 1.657e$, where c is the water vapour content in mm and e is the surface vapour pressure in hPa; $R^2 = 0.94$) (Hu et al., 2015), the surface vapour pressure of each site was used to calculate the value of F.

4 Results and analysis

4.1 Hydrogen and oxygen isotope variations in different waterbodies

During the growth season of *Picea crassifolia*, precipitation stable isotopes display distinct fluctuation patterns (Table 2). In the initial growth phase, the hydrogen and oxygen isotope ratios exhibit relatively low values. With the progressive rise in temperature, the rate of water evaporation and subsequent loss escalates, resulting in isotopic enrichment. The mean δ^2H value in precipitation throughout the growth season is recorded at −45.52 ‰, with fluctuations ranging from −151.88 ‰ to 63.43 ‰. Similarly, the mean δ^{18}O value stands at −7.75 ‰, exhibiting fluctuations between −31.49 ‰ and 14.79 ‰. The isotopic composition in the wood tissues does not show significant depletion or enrichment, displaying a fluctuation range from −76.95 ‰ to 23.87 ‰ for δ^2H and from −11.92 ‰ to 24.77 ‰ for δ^{18}O. Compared to precipitation and wood tissues, shallow soil water demonstrates a lesser enrichment of heavy isotopes, with a reduced fluctuation extent observed during the late spring and early summer period.

Using the global meteoric water line (GMWL) as a reference standard, regional water lines are influenced by factors like moisture source and re-evaporation during precipitation. The intersection points of the local meteoric water line (LMWL), soil water line (SWL), and local evaporation line (LEL) can reveal recharge relationships between different waterbodies. Their slopes reflect key information including local temperature and humidity characteristics, as well as the degree of evaporative fractionation in waterbodies. Variations in the local meteoric water line (LMWL) across different vertical gradients are primarily influenced by temperature and humidity. Notably, relative humidity remains consistently low at all four measured elevations within the forest, causing the LMWL to be lower than the global meteoric water line (GMWL). At an elevation of 2543 m, which marks the lowest tree growth layer, temperatures can reach up to 20 °C in July, with the LMWL showing a slope of 6.74. At 2721 m, the average temperature during the growing season is 10.4 °C, peaking at 16.45 °C in July, with an average relative humidity of 64.38 %. The slope of the LMWL at this elevation is 7.02 (Fig. 2d). At the Suidao station, located at an elevation of 3448 m, the slope of the precipitation regression line is 7.75. This value is close to the GMWL's slope but exhibits the largest deviation from the local evaporation line, as depicted in (Fig. 2a). In the forest's lower layer, the soil water line (SWL) is narrower and closer to the local evaporation line, indicating more pronounced evaporative fractionation and dynamic fractionation compared to the other three sampling zones. The SWL slopes are less steep than those of the LMWL, indicating that precipitation is the primary source of soil moisture replenishment.

The d-excess parameter measures how much precipitation deviates from the global meteoric water line, reflecting the impact of re-evaporation on isotope fractionation. Higher d-excess values indicate stronger non-equilibrium evaporation during regional moisture transport. During the precipitation process, unsaturated water vapour leads to non-equilibrium fractionation, as indicated by an average d-excess value of 16.58 ‰ throughout the growing season (Fig. 3a). Lower relative humidity in May and September results in higher d-excess values compared to other months, indicating more pronounced non-equilibrium evaporation during precipitation events. From June to August, the fluctuations in deuterium values are gradual; however, significant variations be-

Table 2. Stable isotopes of different waterbodies during the growing season.

Average	δ^2H (‰$^{-1}$)			δ^{18}O (‰$^{-1}$)		
Period	Precipitation	Xylem water	Soil water (0–10 cm)	Precipitation	Xylem water	Soil water (0–10 cm)
April	−69.15	−39.02	−53.10	−10.25	2.56	−7.10
May	−39.09	−29.78	−45.38	−7.61	4.44	−6.42
June	−31.29	−45.83	−46.08	−5.74	−2.83	−6.12
July	−32.39	−47.63	−47.71	−5.33	−0.97	−7.06
August	−48.88	−44.55	−68.85	−7.79	−2.06	−9.07
September	−29.38	−42.62	−49.20	−6.46	−1.83	−6.79
October	−68.43	−44.57	−54.88	−11.06	−2.25	−7.96

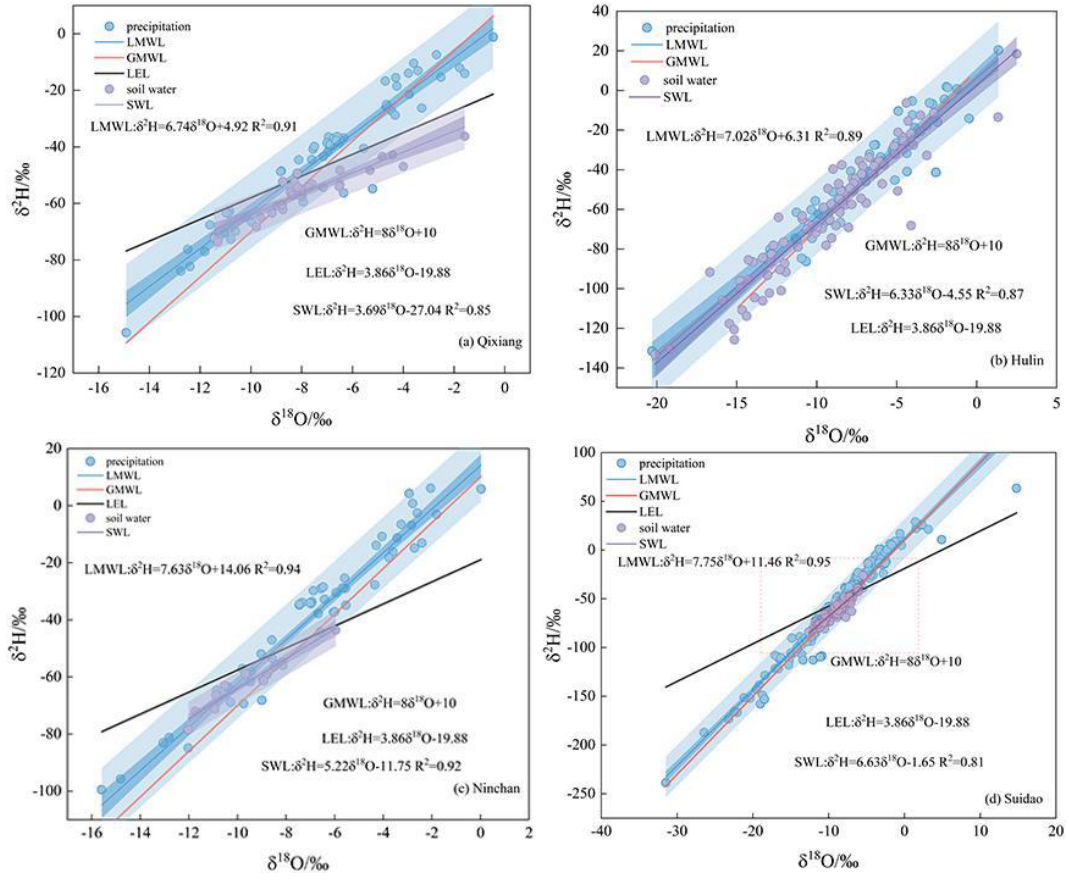

Figure 2. The distributions and fittings of precipitation and soil water stable isotopes at **(a)** Qixiang, **(b)** Hulin, **(c)** Ninchan, and **(d)** Suidao.

gin from mid-August onwards. This trend suggests that local evaporation intensifies over time, influenced by temperature and relative humidity, resulting in increased rates of non-equilibrium evaporation. At higher elevations, the soil moisture content across all soil layers remains above 30 %, influenced by rainfall and snowmelt (Fig. 3b). By the end of the growing season, decreasing temperatures lead to leaf fall, resulting in the formation of a litter layer on the forest floor. This layer plays a pivotal role in retaining soil moisture, underscoring the dynamic interactions between vegetation, soil, and atmospheric conditions throughout the season.

4.2 Soil evaporation, plant transpiration, and ecosystem evapotranspiration

The Keeling plot method was used to analyse the stable isotope composition of ecosystem evapotranspiration (Fig. 4). Its principle involves linearly fitting the water vapour concentration in the ecosystem boundary layer to the oxygen isotope composition, with the intercept on the y axis representing the

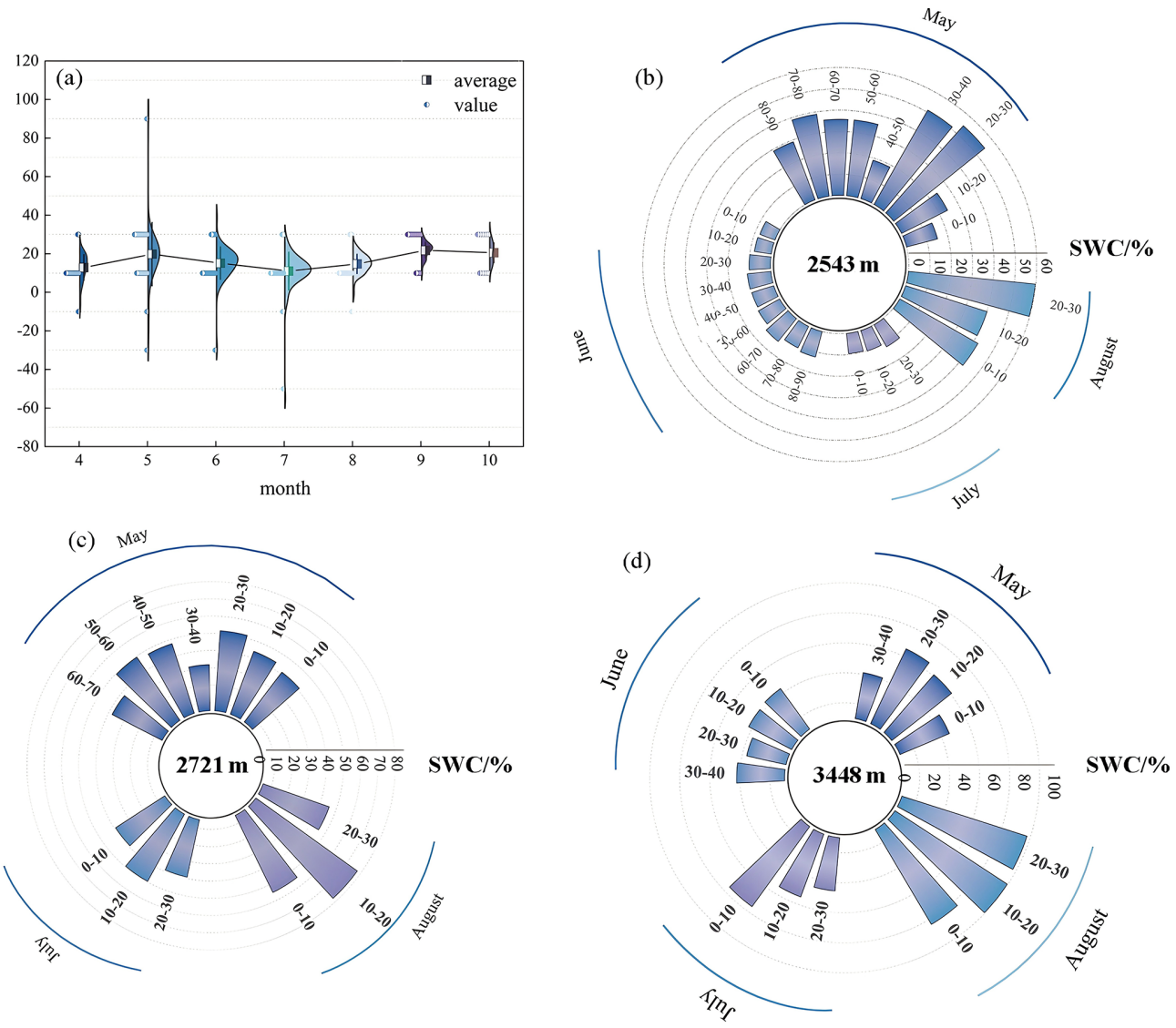

Figure 3. **(a)** The average variation in d-excess during the growing season within the gradient of 2543 to 3448 m; panels **(b)**, **(c)**, and **(d)** represent the soil water content (SWC) at different depths at elevations of 2543, 2721, and 3448 m, respectively.

stable isotope value of δ_{ET}. The results indicate that at different heights within the distribution of deciduous trees, the average δ_{ET} value is $-22.59\,‰$. Throughout the entire growing season, δ_{ET} does not consistently decrease with increasing elevation. Specifically, near the treeline, there are higher stable isotope values, but in the middle and upper layers of the forest, there is a minimal value, indicating lower and less stable isotopic fractionation in that layer. At an elevation of 3448 m, as the number of deciduous trees decreases and shrubs become dominant, the δ_{ET} value is $-21.81\,‰$ (Table 3). We found that the stable isotope δ_E of soil evaporation at depths of 0–10 cm is more enriched at lower elevations, particularly in April and May when the isotopic enrichment is more pronounced. From June to August, due to a significant increase in vegetation coverage, soil evaporation intensity decreases. In the early stage of the growing season, when leaves have not fully developed, the stable isotope composition of the xylem exhibits a relatively depleted characteristic. In July and August, when leaves are fully expanded, temperatures rise, and the rainy season in mountainous areas commences, transpiration becomes more intense.

4.3 *T* / ET assessment of the *Picea crassifolia* ecosystem in different months

We found that the canopy closure of deciduous trees significantly influences the evapotranspiration of the entire ecosystem (Fig. 5). In April and May, as temperatures rise, surface vegetation exhibits weaker growth, resulting in a higher proportion of soil evaporation within the ecosystem, while

Table 3. The isotopic composition of vegetation transpiration (δ_T), soil evaporation (δ_E), and ecosystem evapotranspiration (δ_{ET}) at different elevations during the growing season (* represents a missing value).

Site	Type	April	May	June	July	August	September	October
Qixiang	δ_T	2.22	−5.87	−4.59	−0.72	−1.72	−1.78	−2.26
	δ_E	−30.32	−28.68	−27.33	−29.12	−28.68	−26.32	−27.27
	δ_{ET}	−20.19	−20.05	−11.63	−9.87	−13.56	−15.85	−21.56
Hulin	δ_T	−5.34	−3.58	−4.13	−0.34	−2.35	−4.25	−1.97
	δ_E	−29.68	−27.28	−25.8	−27.75	−24.56	−25.21	−27.88
	δ_{ET}	−21.59	−22.36	−8.93	−10.17	−11.57	−18.8	*
Ninchan	δ_T	*	−3.45	−1.98	−1.05	−6.68	*	*
	δ_E	*	−20.57	−26.31	−29.08	−18.22	−18.15	−18.22
	δ_{ET}	*	*	−12.46	−7.57	*	*	*
Suidao	δ_T	*	−8.45	−6.98	−6.05	−6.68	*	*
	δ_E	−29.79	−27.32	−27.91	−23.83	−28.78	−25.8	−28.06
	δ_{ET}	−24.31	−16.14	−15.19	−10.07	−18.05	−23.02	−18.65

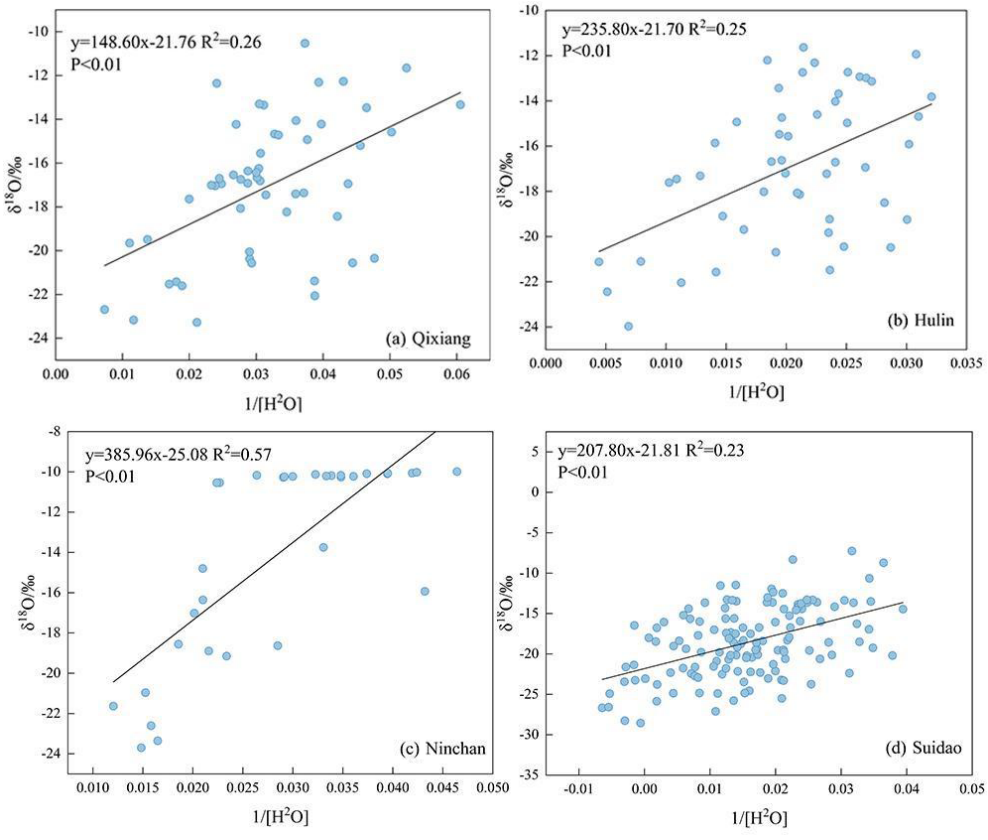

Figure 4. Each sampling point is fitted with a trend line based on the Keeling plot method.

transpiration by vegetation remains relatively low. During the rainy season in June to August, vegetation experiences vigorous growth, and transpiration reaches its peak in July. In September and October, soil evaporation becomes more dominant as temperatures, relative humidity, and rainfall gradually decrease, and deciduous tree leaves become wilted. At lower elevations, the T / ET ratio fluctuates between 0.20 and 0.70 in a different pattern, while above the treeline, transpiration ratios fluctuate between 0.20 and 0.80 in a similar pattern. Overall, summer is characterized as the peak season for transpiration, with a minimal contribution from soil evaporation.

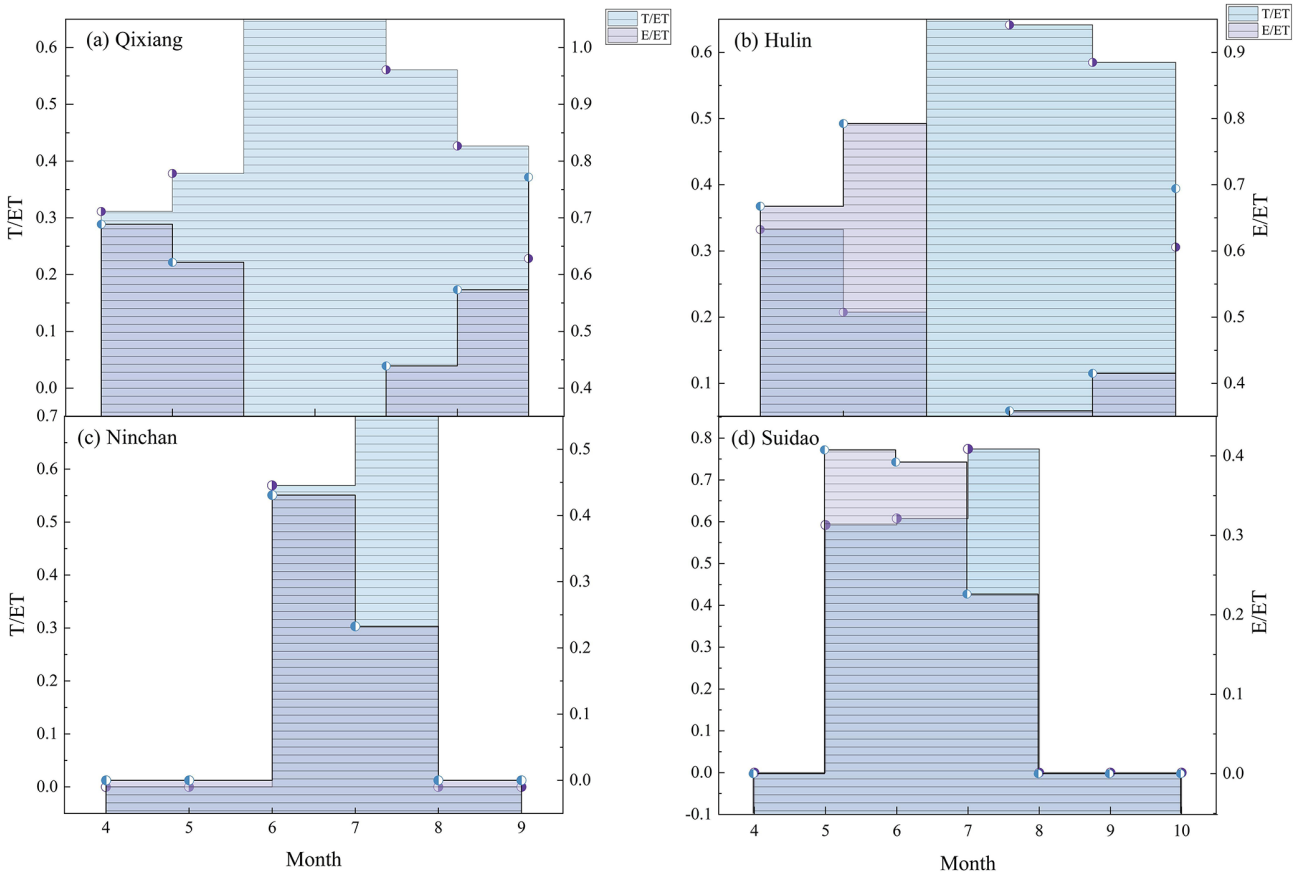

Figure 5. Panels **(a)**, **(b)**, **(c)**, and **(d)** represent the proportion of soil evaporation and vegetation transpiration in the evapotranspiration of the ecosystem at different sampling points (0 represents a missing value).

5 Discussions

5.1 Hydrological effects of changes in evapotranspiration

5.1.1 Contribution to recirculating water vapour in precipitation

The analysis results indicate that the proportion of vegetation in ecosystem evapotranspiration and recycled water vapour is significantly greater than that of the soil. Furthermore, the enhanced evapotranspiration capacity accelerates the cycling rate of water vapour, promoting precipitation formation. Within the altitude gradient of 2700–3000 m, the contribution of advected water vapour gradually declines (Table S2), while the contribution ratio of recycled water vapour to precipitation gradually increases (Fig. 6). This is attributed to relatively high temperatures in the lower layers of the forest and the dense presence of *Picea crassifolia* in the middle to upper layers, resulting in a higher transpiration ratio (f_{tr}) throughout the entire growing season. In July, which typically experiences higher temperatures and increased vegetation activity, the ratio of vegetation transpiration (f_{tr}) is significantly higher compared to other months. Both the early and the late stages of the growing season exhibit noticeably higher evaporation ratios (f_{ev}) compared to other months, with the middle and upper parts of the forest having a greater proportion of evaporated vapour. The average advected vapour ratio (f_{adv}) is 72 %, with contributions exceeding 70 % for all months except June and July. In mountainous areas, recycled water vapour contributes an average of 28 % to precipitation, indicating that the increase in evapotranspiration promotes the occurrence of local precipitation events. This also means that cross-regional water vapour transport and local-scale recycled water vapour alleviate regional water resource crises and enhance the ecosystem's resilience to drought by regulating the redistribution of precipitation and surface water (Quan et al., 2024).

5.1.2 Impact on surface runoff

The formation of runoff is regulated by elevation. In the distribution area of *Picea crassifolia*, the level of evapotranspiration is much higher than precipitation, making it difficult for surface runoff to form (Table 4). However, to support forest growth and maintain the regional water balance, up-

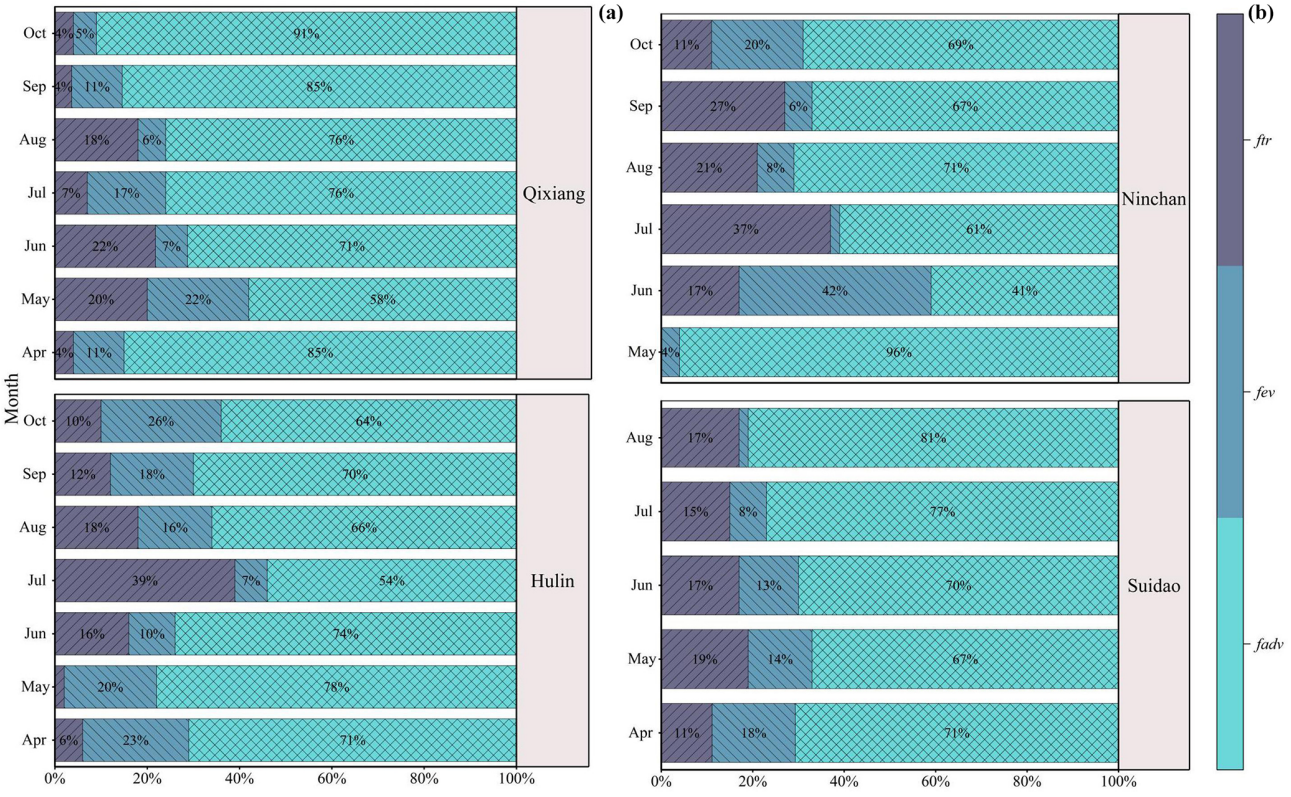

Figure 6. Comparison of f_{adv} (advective water vapour contribution), f_{ev} (surface evaporation water vapour contribution), and f_{tr} (plant transpiration water vapour contribution) for each period.

stream snowmelt compensates for the deficit between precipitation and evapotranspiration and flows into the forest ecosystem as a supplemental water source. Between 2500 and 3400 m, *Picea crassifolia*-dominated forests cover approximately 38.5 % of the watershed area. However, such vegetation exerts only a minor influence on total annual runoff (He et al., 2011). With rising temperatures, precipitation becomes the primary water source for these forests, whereas during dry and cold seasons, snowmelt and seasonal permafrost are integral for both forest water supply and baseflow formation. Seasonal permafrost above 3000 m shapes baseflow from November through April. Over the growing season (2700–3400 m), rainfall is the governing factor behind runoff dynamics (Liu et al., 2023), and snowmelt accounts for 33 % of the water absorbed by *Picea crassifolia* (Zhu et al., 2022b). Overall, forests at mid-elevations rely largely on rainfall and secondarily on meltwater and seasonal permafrost, while their ability to intercept rainwater for runoff generation is relatively limited. Notably, the thickness of seasonal permafrost in this region has declined by 7.4 cm per decade (Qin et al., 2016), further restricting its influence on runoff. From this, an important conclusion can be drawn: at elevations between 2500 and 3400 m, local evapotranspiration substantially exceeds precipitation. Regional runoff is predominantly sustained by precipitation, with forest interception and seasonal permafrost having limited effects on runoff. The feeble runoff generation potential in this region also indicates that afforestation would significantly increase water loss via ET, posing a threat to water distribution and utilization.

Some studies have suggested that reducing forest density will result in less ET in seasonally dry forests. That reduced ET can be converted into increased groundwater and runoff to supply downstream social water (Wyatt et al., 2014). It has also been claimed that in some cases, the transient increase in water availability through reduced forest density can actually contribute to subsequent increases in vegetation cover and ultimately reduce runoff (Tague et al., 2019). By assessing the hydrological effects of afforestation through the water cycle in the Asia–Pacific region, it was found that in 7 of 15 water-deficient areas, positive effects such as increased yield, precipitation, and soil moisture and reduced drought risk were achieved through afforestation, and it was confirmed that the water–water cycle had a strong impact and evapotranspiration was increased (Teo et al., 2022). The water vapour content produced by forest transpiration is much higher than that lost by soil surface evaporation; most of the precipitation is intercepted and infiltrated by surface vegetation, and part of the soil water involved in infiltration is absorbed by the root zone of vegetation. Because of plants' high interception

Table 4. Variations in evapotranspiration (ET) and precipitation (P) across different elevation zones during April to October.

Altitude (m)	Parameter	April	May	June	July	August	September	October	Data source
2700	ET (mm)	51.5	66.3	93.3	108.9	110.7	81.2	41.8	Yao et al. (2020)
2700	P (mm)	29	31.2	103.5	90.3	66.9	39.3	10.4	Zhao et al. (2019, 2020)
3200	ET (mm)	37.5	90	95	107.5	107.5	65	65	Yang et al. (2019)
3200	P (mm)	27.9	43.9	62.3	39.4	56.6	42.7	23.6	Zhao et al. (2021, 2022)

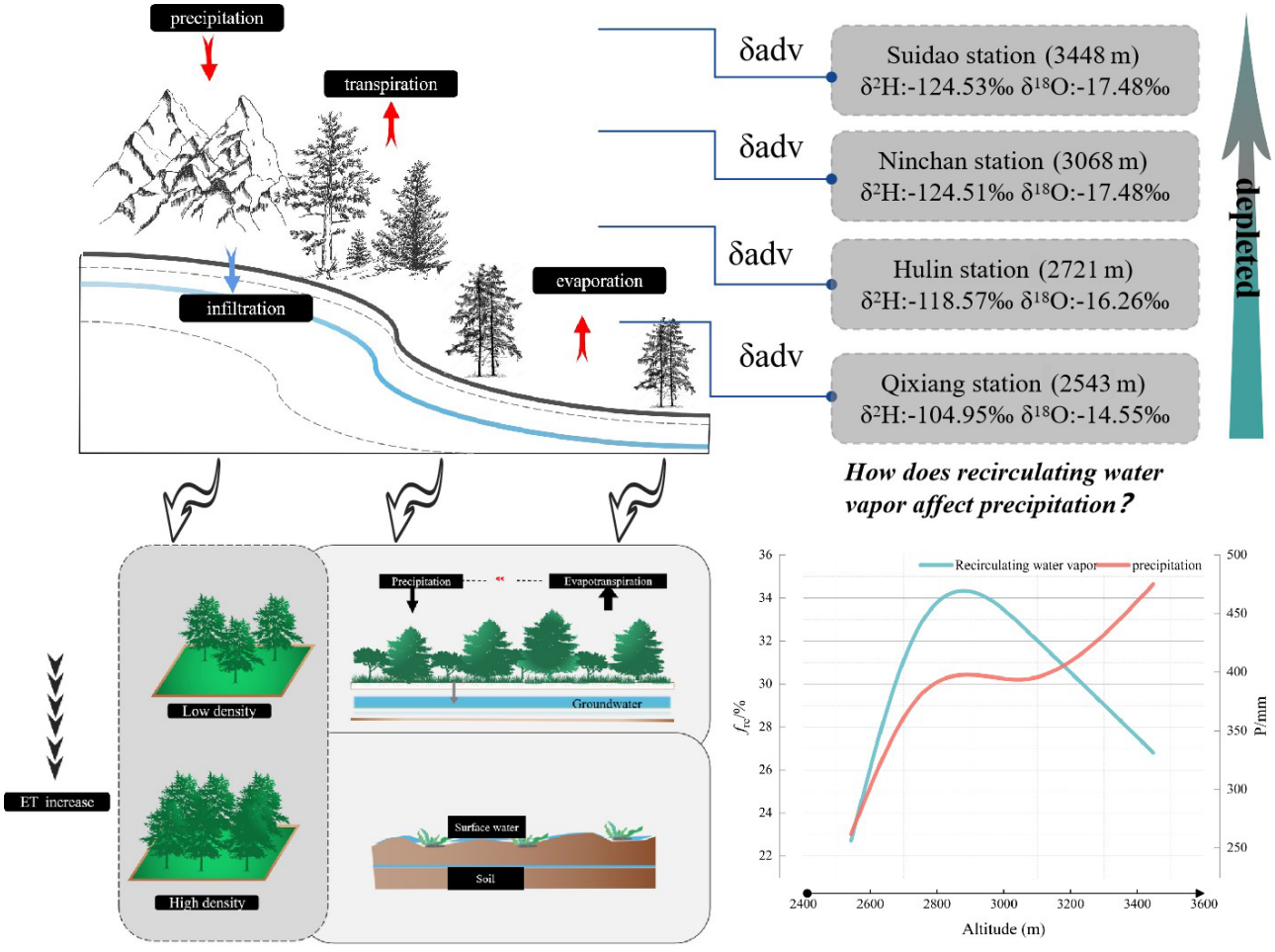

Figure 7. Conceptual model of the hydrological effects of changes in evapotranspiration.

and evaporation ability and the absorption of groundwater by the root zone, the proportion of transpiration was significantly higher than that of evaporation (Sun et al., 2019). In this study zone, upwardly transported advective water vapour progressively diminishes with increasing altitude. The vegetation at elevations from 2500 to 3200 m supplies abundant evapotranspiration water vapour into the water cycle, the acceleration of which boosts local precipitation (Fig. 7). Within the elevation range of 2543 to 3448 m, precipitation and seasonal permafrost are the main sources of groundwater recharge. Over the past 55 years, the seasonal permafrost has decreased at a rate of about 7.4 cm per decade (Li et al., 2016). Correlation analysis shows that when seasonal permafrost decreases, soil moisture in the upper layer increases (Qin et al., 2016). As vegetation transpiration increasingly consumes precipitation, soil water, and groundwater, the remaining groundwater becomes more limited. Consequently, within this elevation range, the contribution of groundwater to runoff formation is minimal.

5.2 Uncertainty analysis

A higher sample size can reduce the margin of error. Therefore, we utilized isotopic data from four sites over a 2-year period to evaluate the model. We used 404 xylem samples

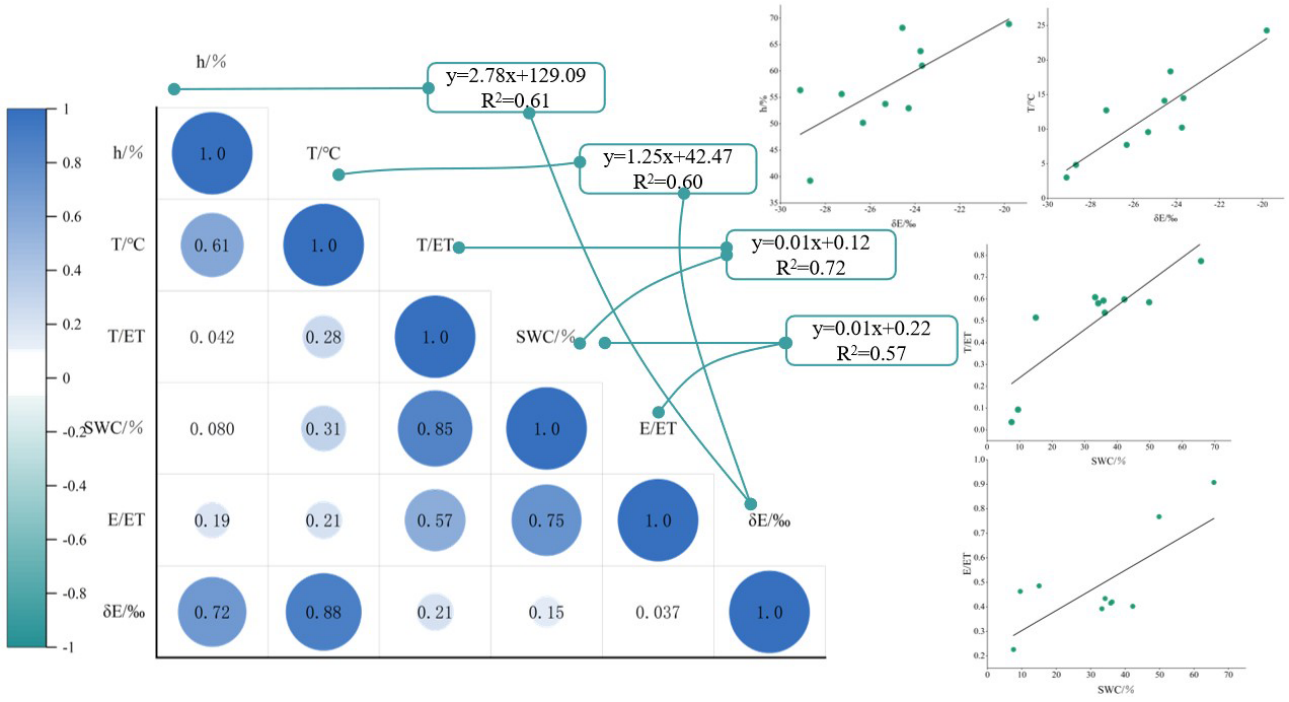

Figure 8. Correlation analysis of factors affecting uncertainty in impact assessment.

to calculate the contribution ratio of transpiration to ecosystem evapotranspiration. We examined the uncertainty in the model evaluation. When analysing the evaporation characteristics in a semi-arid natural environment using the Craig–Gordon isotopic model, we first eliminated the influence of solar radiation and other meteorological variables on the calculation results. We focused on temperature, relative humidity, water vapour, and the initial isotopic values of waterbodies. Particularly in semi-arid environments, the variations in temperature and relative humidity are crucial (Hernández-Pérez et al., 2020). To verify the calculation results, we found a strong correlation between the isotopes of soil evaporation and relative humidity, as demonstrated by the fitting of δ_E against relative humidity and temperature (Fig. 8). This also indicates the reliability of the results obtained through the Craig–Gordon isotopic model. We employed the Keeling plot method to calculate δ_{ET}, which is based on isotopic mass balance and a two-end-member mixing model. This method assumes that the isotopic composition of the background atmosphere and source remains constant, with a very low probability of isotopic spatial variation (Good et al., 2012; Kool et al., 2014). Due to the higher reliability of oxygen isotopes compared to hydrogen isotopes (Han et al., 2022; Celik et al., 2022), we solely used oxygen isotopes to calculate the T / ET values. The results indicate that transpiration significantly outweighs evaporation during July and August, which aligns with previous research findings (Zhu et al., 2022a). The correlation between T / ET and soil moisture content suggests that soil moisture is a crucial factor driving the variations in transpiration and evaporation ratios. Additionally, the estimation of isotopic composition of advected water vapour from the upwind sites contributes to increased uncertainty. In our study area, the sites are predominantly influenced by valley winds, with water vapour moving from the valley bottom to higher altitudes. Therefore, we selected lower-elevation areas in the valley bottom as the source region for advected water vapour (Zhang et al., 2021).

6 Conclusions

This study leverages isotopic data from field observations (2018–2022) and model simulations to investigate the dynamics of evapotranspiration in the northeastern Qinghai–Tibet Plateau, aiming to elucidate its relationship with local water cycling and hydrological impacts. The findings reveal that evaporation and transpiration rates peak during July and August, indicating that transpiration from *Picea crassifolia* plays a more dominant role than soil evaporation in these periods. Quantitative analysis of plant transpiration and soil evaporation contributions to total evapotranspiration yielded an average T / ET ratio of 0.57 over the study period, reaching a maximum of 0.77 in July. Consequently, it is evident that transpiration by forest trees is the primary component of evapotranspiration within the *Picea crassifolia* ecosystem. Further examination of the hydrological effects associated with *Picea crassifolia* evapotranspiration demonstrates that monthly evapotranspiration volumes are at least 3-fold

higher than precipitation, significantly limiting the potential for surface runoff formation in this region. Comparative analysis of atmospheric water vapour contributions from precipitation across spring, summer, and autumn reveals that the June–August period marks the peak transpiration season for *Picea crassifolia*, contributing up to 25 % of total atmospheric water vapour, whereas surface evaporation accounts for only 18 %. Within the 2543 to 3448 m elevation range, the average value of f_{re} is 28 %; it is indicated that the water vapour cycle generated by vegetation evapotranspiration has increased the total precipitation in high-altitude mountain areas. In light of global warming, drought, water scarcity, and climate changes driven by relative humidity, alterations have significantly impacted the ecological communities, ecosystem functions, services, and land–climate interactions of *Picea crassifolia*. It is imperative to recognize the critical role of evapotranspiration in depleting rainfall within this forest belt, underscoring its significance for local water resource management and ecological conservation.

Data availability. The data that support the findings of this study are available on request from the corresponding author; stable isotope data are not publicly available due to privacy or ethical restrictions. Precipitation and surface evapotranspiration data are available from the National Tibetan Plateau Scientific Data Centre (TPDC).

Supplement. The supplement related to this article is available online at https://doi.org/10.5194/bg-22-4433-2025-supplement.

Author contributions. YJ and GZ conceived the idea of the study; GM and SL analysed the data; DQ, QW, RL, and LC participated in the drawing of figures; YJ wrote the paper; WL checked the format. All authors discussed the results and revised the manuscript.

Competing interests. The contact author has declared that none of the authors has any competing interests.

Disclaimer. Publisher's note: Copernicus Publications remains neutral with regard to jurisdictional claims made in the text, published maps, institutional affiliations, or any other geographical representation in this paper. While Copernicus Publications makes every effort to include appropriate place names, the final responsibility lies with the authors.

Acknowledgements. We would like to express our gratitude to the Cold and Arid Research Network (CARN) of Lanzhou University for providing the series of precipitation data that supported some of the research results; these datasets are provided by the National Tibetan Plateau/Third Pole Environment Data Center (http://data.tpdc.ac.cn, last access: 24 April 2025).

Financial support. This research has been supported by the National Natural Science Foundation of China (grant nos. 42371040 and 41971036).

Review statement. This paper was edited by Anja Rammig and reviewed by two anonymous referees.

References

An, Q., Liu, L., Wang, L., Yang, K., Cheng, Y., Liu, J., and Huang, G.: Contribution of moisture recycling to water availability in China, Water Resour. Res., 61, e2024WR038054, https://doi.org/10.1029/2024wr038054, 2025.

Aron, P. G., Poulsen, C. J., Fiorella, R. P., Matheny, A. M., and Veverica, T. J.: An isotopic approach to partition evapotranspiration in a mixed deciduous forest, Ecohydrology, 13, e2229, https://doi.org/10.1002/eco.2229, 2020.

Ault, T. R.: On the essentials of drought in a changing climate, Science, 368, 256–260, https://doi.org/10.1126/science.aaz5492, 2020.

Brubaker, K. L., Entekhabi, D., and Eagleson, P. S.: Estimation of continental precipitation recycling, J. Climate, 6, 1077–1089, https://doi.org/10.1175/1520-0442(1993)006<1077:EOCPR>2.0.CO;2, 1993.

Celik, S. K., Madenoglu, S., and Turker, U.: Partitioning evapotranspiration of winter wheat based on oxygen isotope approach under different irrigation regimes, Irrig. Drain., 71, 882–896, https://doi.org/10.1002/ird.2701, 2022.

Cheng, T. F., Chen, D., Wang, B., Ou, T., and Lu, M.: Human-induced warming accelerates local evapotranspiration and precipitation recycling over the Tibetan Plateau, Commun. Earth Environ., 5, 388, https://doi.org/10.1038/s43247-024-01563-9, 2024.

Craig, H. and Gordon, L. I.: Deuterium and oxygen 18 variations in the ocean and the marine atmosphere, in: Proc. Stable Isotopes in Oceanographic Studies and Paleotemperatures, Spoleto, Italy, edited by: Tongiogi, E., V. Lishi e F., Pisa, Italy, 9–130, 1965.

Cui, J., Lian, X., Huntingford, C., Gimeno, L., Wang, T., Ding, J., He, M., Xu, H., Chen, A., Gentine, P., and Piao, S.: Global water availability boosted by vegetation-driven changes in atmospheric moisture transport, Nat. Geosci., 15, 982–988, https://doi.org/10.1038/s41561-022-01061-7, 2022.

Dansgaard, W.: Stable isotopes in precipitation, Tellus, 16, 436–468, https://doi.org/10.1111/j.2153-3490.1964.tb00181.x, 1964.

Eisenhauer, N. and Weigelt, A.: Ecosystem effects of environmental extremes, Science, 374, 1442–1443, https://doi.org/10.1126/science.abn1406, 2021.

Farquhar, G. D., Cernusak, L. A., and Barnes, B.: Heavy water franctionation during transpiration, Plant Physiol., 143, 11–18, https://doi.org/10.1104/pp.106.093278, 2007.

Gibson, J. J. and Reid, R.: Stable isotope fingerprint of open-water evaporation losses and effective drainage area fluctuations in a subarctic shield watershed, J. Hydrol., 381, 142–150, https://doi.org/10.1016/j.jhydrol.2009.11.036, 2009.

Gibson, J. J. and Reid, R.: Water balance along a chain of tundra lakes: A 20-year isotopic perspective, J. Hydrol., 519, 2148–2164, https://doi.org/10.1016/j.jhydrol.2014.10.011, 2014.

Good, S. P., Soderberg, K., Wang, L., and Caylor, K. K.: Uncertainties in the assessment of the isotopic composition of surface fluxes: A direct comparison of techniques using laser-based water vapor isotope analyzers, J. Geophys. Res.-Atmos., 117, D15301, https://doi.org/10.1029/2011jd017168, 2012.

Han, J., Tian, L., Cai, Z., Ren, W., Liu, W., Li, J., and Tai, J.: Season-specific evapotranspiration partitioning using dual water isotopes in a Pinus yunnanensis ecosystem, southwest China, J. Hydrol., 608, 127672, https://doi.org/10.1016/j.jhydrol.2022.127672, 2022.

Hao, L., Sun, G., Huang, X., Tang, R., Jin, K., Lai, Y., Chen, D., Zhang, Y., Zhou, D., Yang, Z.-L., Wang, L., Dong, G., and Li, W.: Urbanization alters atmospheric dryness through land evapotranspiration, npj Clim. Atmos. Sci., 6, 149, https://doi.org/10.1038/s41612-023-00479-z, 2023.

He, Z., Zhao, W., Liu, H., and Tang, Z.: Effect of forest on annual water yield in the mountains of an arid inland river basin: a case study in the Pailugou catchment on northwestern China's Qilian Mountains, Hydrol. Process., 26, 613–621, https://doi.org/10.1002/hyp.8162, 2011.

Hernández-Pérez, E., Levresse, G., Carrera-Hernández, J., and García-Martínez, R.: Short term evaporation estimation in a natural semiarid environment: New perspective of the Craig – Gordon isotopic model, J. Hydrol., 587, 124926, https://doi.org/10.1016/j.jhydrol.2020.124926, 2020.

Horita, J. and Wesolowski, D. J.: Liquid-vapor fractionation of oxygen and hydrogen isotopes of water from the freezing to the critical temperature, Geochim. Cosmochim. Ac., 58, 3425–3437, https://doi.org/10.1016/0016-7037(94)90096-5, 1994.

Hu, W.-F., Yao, J.-Q., He, Q., and Yang, Q.: Spatial and temporal variability of water vapor content during 1961–2011 in Tianshan Mountains, China, J. Mt. Sci., 12, 571–581, https://doi.org/10.1007/s11629-014-3364-y, 2015.

Keeling, C. D.: The concentration and isotopic abundances of atmospheric carbon dioxide in rural areas, Geochim. Cosmochim. Ac., 13, 322–334, https://doi.org/10.1016/0016-7037(58)90033-4, 1958.

Kong, Y., Pang, Z., and Froehlich, K.: Quantifying recycled moisture fraction in precipitation of an arid region using deuterium excess, Tellus B, 65, 19251, https://doi.org/10.3402/tellusb.v65i0.19251, 2013.

Kool, D., Agam, N., Lazarovitch, N., Heitman, J. L., Sauer, T. J., and Ben-Gal, A.: A review of approaches for evapotranspiration partitioning, J. Adv. Res., 184, 56–70, https://doi.org/10.1016/j.agrformet.2013.09.003, 2014.

Li, X. and Zhang, G.: Research on Precipitable Water and Precipitation Conversion Efficiency around Tianshan Mountain Area, J. Desert Res., 23, 509–513, 2003.

Li, Z., Feng, Q., Wang, Q. J., Song, Y., Li, H., and Li, Y.: The influence from the shrinking cryosphere and strengthening evopotranspiration on hydrologic process in a cold basin, Qilian Mountains, Glob. Planet. Change, 144, 119–128, https://doi.org/10.1016/j.gloplacha.2016.06.017, 2016.

Li, Z., Ciais, P., Wright, J. S., Wang, Y., Liu, S., Wang, J., Li, L. Z. X., Lu, H., Huang, X., Zhu, L., Goll, D. S., and Li, W.: Increased precipitation over land due to climate feedback of large-scale bioenergy cultivation, Nat. Commun., 14, 4096, https://doi.org/10.1038/s41467-023-39803-9, 2023.

Liu, Z., Wang, N., Cuo, L., and Liang, L.: Characteristics and attribution of spatiotemporal changes in Qilian Mountains' runoff over the past six decades, J. Geophys. Res.-Atmos., 128, e2023JD039176, https://doi.org/10.1029/2023jd039176, 2023.

Makarieva, A. M., Nefiodov, A. V., Nobre, A. D., Baudena, M., Bardi, U., Sheil, D., Saleska, S. R., Molina, R. D., and Rammig, A.: The role of ecosystem transpiration in creating alternate moisture regimes by influencing atmospheric moisture convergence, Glob. Change Biol., 29, 2536–2556, https://doi.org/10.1111/gcb.16644, 2023.

Mehmood, S., Ashfaq, M., Kapnick, S., Gosh, S., Abid, M. A., Kucharski, F., Batibeniz, F., Saha, A., Evans, K., and Hsu, H.-H.: Dominant controls of cold-season precipitation variability over the high mountains of Asia, npj Clim. Atmos. Sci., 5, 65, https://doi.org/10.1038/s41612-022-00282-2, 2022.

Peng, T., Liu, K., Wang, C., and Chuang, K.: A water isotope approach to assessing moisture recycling in the island-based precipitation of Taiwan: A case study in the western Pacific, Water Resour. Res., 47, W08507, https://doi.org/10.1029/2010wr009890, 2011.

Phillips, D. L. and Gregg, J. W.: Uncertainty in source partitioning using stable isotopes, Oecologia, 127, 171–179, https://doi.org/10.1007/s004420000578, 2001.

Qin, Y., Lei, H., Yang, D., Gao, B., Wang, Y., Cong, Z., and Fan, W.: Long-term change in the depth of seasonally frozen ground and its ecohydrological impacts in the Qilian Mountains, northeastern Tibetan Plateau, J. Hydrol., 542, 204–221, https://doi.org/10.1016/j.jhydrol.2016.09.008, 2016.

Quan, Q., He, N., Zhang, R., Wang, J., Luo, Y., Ma, F., Pan, J., Wang, R., Liu, C., Zhang, J., Wang, Y., Song, B.,Li, Z., Zhou, Q., Yu, G., and Niu, S.: Plant height as an indicator for alpine carbon sequestration and ecosystem response to warming. Nat. Plants, 10, 890–900, https://doi.org/10.1038/s41477-024-01705-z, 2024.

Raz-Yaseef, N., Rotenberg, E., and Yakir, D.: Effects of spatial variations in soil evaporation caused by tree shading on water flux partitioning in a semi-arid pine forest, Agr. Forest Meteorol., 150, 454–462, https://doi.org/10.1016/j.agrformet.2010.01.010, 2010.

Sang, L., Zhu, G., Xu, Y., Sun, Z., Zhang, Z., and Tong, H.: Effects of agricultural Large-And Medium-Sized reservoirs on hydrologic processes in the arid Shiyang River basin, northwest China, Water Resour. Res., 59, e2022WR033519, https://doi.org/10.1029/2022wr033519, 2023.

Skrzypek, G., Mydłowski, A., Dogramaci, S., Hedley, P., Gibson, J. J., and Grierson, P. F.: Estimation of evaporative loss based on the stable isotope composition of water using Hydrocalculator, J. Hydrol., 523, 781–789, https://doi.org/10.1016/j.jhydrol.2015.02.010, 2015.

Stein, A. F., Draxler, R. R., Rolph, G. D., Stunder, B. J. B., Cohen, M. D., and Ngan, F.: NOAA's HYSPLIT Atmospheric Transport and Dispersion Modeling system, B. Am. Meteorol. Soc., 96, 2059–2077, https://doi.org/10.1175/bams-d-14-00110.1, 2015.

Sun, X., Wilcox, B. P., and Zou, C. B.: Evapotranspiration partitioning in dryland ecosystems: A global meta-analysis of in situ studies, J. Hydrol., 576, 123–136, https://doi.org/10.1016/j.jhydrol.2019.06.022, 2019.

Tague, C. L., Moritz, M., and Hanan, E.: The changing water cycle: The eco-hydrologic impacts of forest density reduction in

Mediterranean (seasonally dry) regions, Wiley Interdiscip. Rev. Water, 6, e1350, https://doi.org/10.1002/wat2.1350, 2019.

Teo, H. C., Raghavan, S. V., He, X., Zeng, Z., Cheng, Y., Luo, X., Lechner, A., Ashfold, M. J., Lamba, A., Sreekar, R., Zheng, Q., Chen, A., and Koh, L. P.: Large-scale reforestation can increase water yield and reduce drought risk for water-insecure regions in the Asia-Pacific, Glob. Change Biol., 28, 6385–6403, https://doi.org/10.1111/gcb.16404, 2022.

Wang, P., Yamanaka, T., Li, X.-Y., and Wei, Z.: Partitioning evapotranspiration in a temperate grassland ecosystem: Numerical modeling with isotopic tracers, Agric. For. Meteorol., 208, 16–31, https://doi.org/10.1016/j.agrformet.2015.04.006, 2015.

Wang, S., Zhang, M., Che, Y., Chen, F., and Qiang, F.: Contribution of recycled moisture to precipitation in oases of arid central Asia: A stable isotope approach, Water Resour. Res., 52, 3246–3257, https://doi.org/10.1002/2015wr018135, 2016.

Wang, S., Wang, L., Zhang, M., Shi, Y., Hughes, C. E., Crawford, J., Zhou, J., and Qu, D.: Quantifying moisture recycling of a leeward oasis in arid central Asia using a Bayesian isotopic mixing model, J. Hydrol., 613, 128459, https://doi.org/10.1016/j.jhydrol.2022.128459, 2022.

Wei, Z., Lee, X., Wen, X., and Xiao, W.: Evapotranspiration partitioning for three agro-ecosystems with contrasting moisture conditions: a comparison of an isotope method and a two-source model calculation, Agric. For. Meteorol., 252, 296–310, https://doi.org/10.1016/j.agrformet.2018.01.019, 2018.

Wyatt, C. J. W., O'Donnell, F. C., and Springer, A. E.: Semi-Arid aquifer responses to forest restoration treatments and climate change, Ground Water, 53, 207–216, https://doi.org/10.1111/gwat.12184, 2014.

Yang, Y., Chen, R., Song, Y., Han, C., Liu, J., and Liu, Z.: Sensitivity of potential evapotranspiration to meteorological factors and their elevational gradients in the Qilian Mountains, northwestern China, J. Hydrol., 568, 147–159, 2019.

Yao, Y., Liu, S., and Shang, K.: Daily MODIS-based Land Surface Evapotranspiration Dataset of 2019 in Qilian Mountain Area (ETHi-merge V1.0), National Tibetan Plateau/Third Pole Environment Data Center [data set], https://doi.org/10.11888/Meteoro.tpdc.270407, 2020.

Yepez, E. A., Huxman, T. E., Ignace, D. D., English, N. B., Weltzin, J. F., Castellanos, A. E., and Williams, D. G.: Dynamics of transpiration and evaporation following a moisture pulse in semiarid grassland: A chamber-based isotope method for partitioning flux components, Agr. Forest Meteorol., 132, 359–376, https://doi.org/10.1016/j.agrformet.2005.09.006, 2005.

Zhang, Z., Zhu, G., Pan, H., Sun, Z., Sang, L., and Liu, Y.: Quantifying recycled moisture in precipitation in Qilian Mountains, Sustainability, 13, 12943, https://doi.org/10.3390/su132312943, 2021.

Zhao, C., Zhang, R., and Wang, Y.: Qilian Mountains integrated observatory network: Cold and Arid Research Network of Lanzhou University (an observation system of meteorological elements gradient of Dayekou Station, 2018), National Tibetan Plateau/Third Pole Environment Data Center [data set], https://doi.org/10.11888/Geogra.tpdc.270169, 2019.

Zhao, C., Zhang, R., and Wang, Y.: Cold and Arid Research Network of Lanzhou university (an observation system of Meteorological elements gradient of Dayekou Station, 2019), National Tibetan Plateau/Third Pole Environment Data Center [data set], https://doi.org/10.11888/Meteoro.tpdc.270799, 2020.

Zhao, C., Zhang, R., and Zhao, C.: Cold and Arid Research Network of Lanzhou university (an observation system of Meteorological elements gradient of Sidalong Station, 2020), National Tibetan Plateau/Third Pole Environment Data Center [data set], https://doi.org/10.11888/Meteoro.tpdc.271378, 2021.

Zhao, C., Zhang, R., and Zhao, C.: Cold and Arid Research Network of Lanzhou university (an observation system of Meteorological elements gradient of Sidalong Station, 2021), National Tibetan Plateau/Third Pole Environment Data Center [data set], https://doi.org/10.11888/Atmos.tpdc.272365, 2022.

Zhu, G., Liu, Y., Shi, P., Jia, W., Zhou, J., Liu, Y., Ma, X., Pan, H., Zhang, Y., Zhang, Z., Sun, Z., Yong, L., and Zhao, K.: Stable water isotope monitoring network of different water bodies in Shiyang River basin, a typical arid river in China, Earth Syst. Sci. Data, 14, 3773–3789, https://doi.org/10.5194/essd-14-3773-2022, 2022a.

Zhu, G., Wang, L., Liu, Y., Bhat, M.A., Qiu, D., Zhao, K., Sang, L., Lin, X., and Ye, L.: Snow-melt water: An important water source for Picea crassifolia in Qilian Mountains, J. Hydrol., 613, 128441, https://doi.org/10.1016/j.jhydrol.2022.128441, 2022b.